



Contents lists available at ScienceDirect

Arabian Journal of Chemistry

journal homepage: www.sciencedirect.com

Original article

Influence of CaCe ratio on the hydrogen production from ammonia over CaO-CeO₂ supported Co catalysts

Seetharamulu Podila*, Abdulrahim A. Al-Zahrani, Nagaraju Pasupulety, Majed A. Alamoudi

Chemical and Materials Engineering Department, Faculty of Engineering, King Abdulaziz University, P.O. Box 80204, Jeddah 21589, Saudi Arabia

ARTICLE INFO

Article history:

Received 6 May 2023

Accepted 31 August 2023

Available online 9 September 2023

Keywords:

CaO-CeO₂ mixed oxide

Hydrogen production

Cobalt and Ammonia decomposition

ABSTRACT

Hydrogen (H₂) fuel has the potential to replace fossil fuel for generating electricity, clean energy and generating power. Ammonia (NH₃) has the potential to overcome the challenges associated with storage, transportation, and use of hydrogen fuel. The catalytic decomposition of ammonia into hydrogen is studied over cobalt catalysts supported on CaO-CeO₂ mixed oxide. The influence of the Ca/Ce ratio in the support composition on catalytic activity was investigated. The CaO-CeO₂ mixed oxide support materials prepared with different Ca/Ce ratios (1:1, 2:1 and 3:1). The overall basicity of catalyst varied with the increase of Ca to CaO-CeO₂ mixed oxide and showed maximum at Ca/Ce = 2. The cobalt catalysts are prepared with a nominal 5 wt% Co over CaO-CeO₂ mixed oxide support with various Ca/Ce ratios. Among all prepared catalysts 5CoCaCe-21 (5 wt%Co on CaO-CeO₂ mixed oxide with Ca/Ce = 2) showed highest activity. Surface area, X-ray diffraction (XRD), Temperature Program Reduction (TPR), Scanning Electron Microscopy (SEM), and CO₂ Temperature Program Desorption (TPD) methods were used to characterize the synthesized materials. The high performance of 5CoCaCe-21 catalyst is due to high basicity, suitable metal support interactions, high surface area and easy reducibility of Co species resulting from its support favorable properties. The effect of cobalt loadings also studied on CaCe-21 support. The 10 wt%Co on CaCe-21 (10CoCaCe-21) showed highest activity among all other cobalt loadings. The 10CoCaCe-21 catalyst showed excellent stability for H₂ production from NH₃ during 70 h of time on study with different GHSV's.

© 2023 The Author(s). Published by Elsevier B.V. on behalf of King Saud University. This is an open access article under the CC BY license (<http://creativecommons.org/licenses/by/4.0/>).

1. Introduction

Hydrogen (H₂) is a clean fuel and it can be produced using a number of different processes with different catalysts (Hafeez et al., 2023a, 2023b). There are challenges preventing H₂ in usage by means of transportation and storage. A high pressure, low-temperature environment is conducive to store H₂ at high density. These conditions increase storage expenses and lead to safety problems due to leakages (Podila et al., 2015, 2016a, Sun et al., 2022). There are solid-state materials that can be used for hydrogen storage, including metal hydrates, which store H₂ at low pres-

ures. It remains a challenge to balance fast kinetics with high storage capacity in these materials. Chemicals such as Ammonia (NH₃), Methane (CH₄), and Methanol (CH₃OH) contain hydrogen and can be used to store hydrogen as well. Only NH₃ has proven to be an effective and secure hydrogen energy carrier among these chemicals (Sun et al., 2022, Podila et al., 2016b). Ammonia has other benefits of well-developed knowledge and infrastructures in terms of storage and transport.

Many metals (Ru, Co, Ni, Fe, Ir, etc.,) have been widely investigated for ammonia splitting among them Ru-based catalysts showed high degree of ammonia conversion (Kim and Park, 2022, Huang et al., 2019, Podila et al., 2017, 2020, Al-attar et al., 2022, Zaman et al., 2018, Cao et al., 2022, Chen et al., 2022, Ohtsuka et al., 2004). As Ru metal is extremely expensive and scarce thus, not to be recommended for real-world practices in fuel cells. Therefore, it is essential to look for a cost-effective alternative such as transitional metallic oxides which are used for many applications (Babu et al., 2023, Madhavi et al., 2021). In addition to metal catalysts, metal amides, metal nitrides and metal carbides

* Corresponding author.

E-mail address: srpodila@kau.edu.sa (S. Podila).

Peer review under responsibility of King Saud University.



have been investigated for ammonia decomposition. The drawbacks of these catalysts are laborious in preparation method and active at higher temperatures only.

Co or Ni-supported catalysts are comparatively low expensive than Ru catalysts and showed fair performance for ammonia decomposition. Hence much attention drawn recently and been considered as alternative catalysts for NH_3 decomposition to produce H_2 . Although nickel is less expensive than cobalt, Ni catalysts requires higher loadings which usually causes severe metal aggregation (Podila et al., 2015, 2022, Chen et al., 2022). Thus, cobalt catalysts are good candidates for ammonia decomposition.

Studies reported in the literature data about the performance of metal-based catalysts on different supports i.e., MgO, Al_2O_3 , SiO_2 , Activated Carbon (AC), meso and microporous materials, Carbon Nanotubes (CNTs) etc. for ammonia decomposition (Ju et al., 2019, 2014, Wu et al., 2020, Li et al., 2017, Chen et al., 2020). Out of all support material, CNTs supported catalysts exhibited excellent performance for H_2 production from NH_3 (Yin et al., 2004a). Methanation and high-priced are the challenges for the usage of CNTs as a support material for this reaction. According to literature reports, a good support for ammonia decomposition should possess the properties of high specific surface area (SSA) and suitable basicity (Yin et al., 2004b). CeO_2 used as the support material for the catalytic ammonia decomposition (Chen et al., 2022). It was reported that the usage of Ceria helps in tuning the support metal interaction because of its oxygen storage and release capacity. Huang et al. (2020) recently studied cobalt catalyst with high surface area CeO_2 as support for ammonia decomposition. On other hand, support basicity is also necessary for efficient catalyst in NH_3 decomposition. The basic property of catalyst strongly influences the electronic state of active metal species which results in the modification of the performance. Thus, better catalyst performance obtains with the strong basicity of the support.

The use of mixed oxide as support can enable the tailoring of a catalyst with proper strength of basicity. Various mixed metal oxide-based catalysts used for many applications such as $\text{MgO-Al}_2\text{O}_3$, $\text{La}_2\text{O}_3\text{-CeO}_2$, $\text{Al}_2\text{O}_3\text{-CeO}_2$ etc., these materials reported also for ammonia decomposition using Ni or Co as active metal. The main drawback with these materials is active at high temperatures. Calcium based catalysts are well known as solid base catalysts for many reactions. However, the Calcium based catalyst is not stable and shows low surface area. To improve the activity and stability of calcium-based catalysts mixed with other metal oxide (CeO_2). Calcium and Cerium based mixed oxides are solid basic catalysts extensively studied in many reactions (Teo et al., 2014, Sivashankar et al., 2022).

To the best of our literature awareness, no reports on the catalytic performance of cobalt on CaO-CeO_2 mixtures for ammonia decomposition have been studied. In this study, we aimed to analyze the cobalt catalysts supported on CaO-CeO_2 mixed oxide for ammonia decomposition. To enhance the interaction of components in support material and alter the basicity of catalyst we prepared a series of CaO-CeO_2 mixed oxides with different Ca/Ce mole ratio. In addition, the present work attempts to study the influence of cobalt loading on optimized CaO-CeO_2 mixed oxide.

2. Experimental

2.1. Chemicals

All chemicals obtained from Merk, Fluka and Aldrich chemicals without any further purification. The chemicals $\text{Ca}(\text{NO}_3)_2 \cdot 6\text{H}_2\text{O}$ (Fluka, 98%), $\text{Ce}(\text{NO}_3)_3 \cdot 6\text{H}_2\text{O}$ (Aldrich, 99.9%), $\text{Co}(\text{NO}_3)_2 \cdot 9\text{H}_2\text{O}$ (Aldrich, 99.9%), CeO_2 (Alfa, 99.5%) CaO (Fluka, 96%) were utilized in catalyst preparation.

2.2. Preparation of CaO-CeO_2 mixed oxides

The support material CaO-CeO_2 mixed oxide was prepared by co-precipitation method using Ca and Ce nitrates with Ca/Ce ratio 1:1. In a standard process, 0.13 mol of $\text{Ca}(\text{NO}_3)_2 \cdot 6\text{H}_2\text{O}$ and 0.13 mol $\text{Ce}(\text{NO}_3)_3 \cdot 6\text{H}_2\text{O}$ were dissolved in deionized water (DH_2O) together in a beaker for a one molar solution. The precipitating agent solution was prepared by dissolving KOH (0.44 mol) and K_2CO_3 (0.12 mol) in DH_2O for 2 M solution. Under conditions of continual stirring, the precipitating agent solution was gradually added to the metal nitrate solution. The precipitation proceeded until the solution's pH reached 11. After precipitation, the mixture was aged for 18 h at 70 °C. The precipitate was then filtered, and the pH was adjusted to 7 by washing with DH_2O . Overnight, the solid was dried at 110 °C. In a muffle furnace, the acquired catalyst was calcined at 450 °C for 18 h. The prepared catalyst denoted as CaCe-11. A similar preparation procedure adapted for mixed oxides with Ca/Ce ratios 2:1 and 3:1 and the prepared supports were recognized as CaCe-21 and CaCe-31.

2.3. Preparation of cobalt catalysts supported on CaO-CeO_2 mixed oxides

The wet impregnation method adapted for the preparation of cobalt catalysts. Calcined CaO-CeO_2 mixed oxide impregnated with aqueous solution of $\text{Co}(\text{NO}_3)_2 \cdot 6\text{H}_2\text{O}$ in a rotary evaporator. The cobalt catalysts impregnated on CaCe-11, CaCe-21 and CaCe-31 supports are labelled as 5CoCaCe-11, 5CoCaCe-21, and 5CoCaCe-31 respectively. For activity comparison, Co catalysts supported on commercial CeO_2 and commercial CaO were prepared which are denoted as 5Co- CeO_2 and 5Co- CaO respectively. The Co loading in all these catalysts were fixed at 5 wt%. After impregnation, all cobalt catalysts were dried at 110 °C overnight. Next the cobalt catalysts were calcined at 500 °C for 18 h in a muffle furnace. The Co loadings with 10 wt%, 15 wt% and 20 wt% catalysts were prepared by impregnation on CaCe-21 support and denoted as 10CoCaCe-21, 15CoCaCe-21 and 20CoCaCe-21 respectively.

2.4. Characterization

The textural properties of the catalysts were derived from N_2 adsorption-desorption isotherms at -196 °C using Nova Station Quanta chrome equipment. Prior to analysis, all the solids were treated under vacuum at 200 °C for 2 h. The specific surface areas and average pore diameters were determined using Brunauer-Emmett-Teller (BET) method.

Using an Inel Equinox 1000 diffractometer, the catalyst's X-ray diffraction (XRD) analysis was documented. A cobalt X-ray tube running at 40 kV and 30 mA with $\text{Co K}\alpha$ radiation ($\lambda = 1.789 \text{ \AA}$). The analysis was performed within a diffraction range between 10 and 115°. Match© Crystal Impact software (v.1.11e) used to process the diffraction results. The PDF database was used to identify the crystalline phases.

An AutoChem 2950 from Micromeritics equipment used to perform Temperature-Programmed Reduction (TPR) analysis with TCD detection. Catalyst (around 0.15 g) was placed in a U-shaped quartz reactor, which was heated to 800 °C at a rate of 10 °C per minute while being reduced with 10% H_2/Ar mixed gas at a flow rate of 50 mL per minute.

CO_2 -temperature programmed desorption ($\text{CO}_2\text{-TPD}$) analysis performed on the same instrument used for TPR analysis. Prior to TPD experiments 0.1 g of calcined catalyst was reduced with 10% H_2/Ar gas at 550 °C for 2 h. Afterwards, the temperature was decreased to 50 °C in He flow and 99.999% CO_2 was flown into the sample bed at same temperature for 1 h. Then, the sample

was purged with He gas and raised the reactor temperature to 900 °C at a ramp rate at 10 °C min⁻¹.

Carbon monoxide chemisorption tests were carried out at 40 °C using AutoChem 2950 Micromeritics equipment. A 100 mg catalyst sample was loaded in a reactor and reduced by pure hydrogen for 2 h at 550 °C. Then the sample was cooled to 40 °C in a helium flow. The adsorption of carbon monoxide was carried by pulse chemisorption method using 10% CO/He mixed gas. The results were calculated assuming the adsorption stoichiometry of CO/Cobalt is 1:1.

The morphologies of the catalysts were examined using a scanning electron microscope (SEM) equipped with an FEI Quanta FEG450 scanning microscope, an ETD (Everhart Thornley detector), and a VCD (back scattering electron detector) unit. Before the SEM examination, a little part of each sample was powder coated on a metallic disk holder and covered in a thin layer of carbon.

2.5. Catalytic performance test

Using 100 mg of catalysts, the ammonia decomposition performance of catalysts was conducted in a fixed-bed quartz micro reactor. The catalyst was activated at 550 °C for 5 h in mixed gases (volume ratio of H₂ to N₂ is 3) before the experiment. The reactor temperature was decreased to a reaction temperature of 300 °C and purged with N₂ gas. The reactor was feed with pure 100% ammonia gas with 6000 h⁻¹ Gas Hour Space Velocity (GHSV). The experiment was carried out at a temperature between 300 and 600 °C with 50 °C-step increases in temperature. After the ammonia decomposition reaction stabilized at each temperature, the data were collected. With the help of a Thermal Conductivity Detector (TCD), the Varian 450 GC was used to evaluate the products and reactants (H₂, N₂, and NH₃).

The following equation was used to calculate the % of NH₃ conversion (X).

$$X = \frac{n_{\text{NH}_3}^i - n_{\text{NH}_3}^o}{n_{\text{NH}_3}^i} \times 100$$

where $n_{\text{NH}_3}^i$ is number of moles/min of NH₃ feed gas at reactor inflow and $n_{\text{NH}_3}^o$ is unconverted moles/min of NH₃ at reactor outflow.

$$\text{H}_2 \text{ formation rate (mmol/g}_{\text{cat}}/\text{min}) = \frac{V_{\text{NH}_3} \cdot \text{Conv}(\text{NH}_3)\% \cdot 1.5}{m_{\text{cat}}}$$

The H₂ formation rate was calculated from the above equation where V_{NH_3} refers to the amount at a flow rate.

3. Results and discussion

3.1. Studies on surface area and pore size distribution

The results of N₂ adsorption–desorption isotherms of the prepared catalysts are shown in Fig. 1 and the corresponding specific surface area (S_{BET}), pore volume (V_{total}) and pore width are summarized in Table 1. The prepared supports showed type IV isotherms, but the shape of the hysteresis loop varied with the change in the ratio of Ca and Ce (Sing, 1985). The calcined CaCe-11 support showed H4 type hysteresis loop that is associated with narrow slit-like pores. Similarly, the support material CaCe-31 showed H4 type hysteresis loop but the gap between adsorption and desorption isotherms are much closer in hysteresis region in CaCe-31 comparison to that of CaCe-11. This indicates condensation in capillary is less due to low pore volume. The H3 type hysteresis loop exhibited by the calcined CaCe-21 support suggests clusters of plate-like particles with slit shaped pores (Sivashankar et al., 2022). Among all synthesized catalysts, the CaCe-11 support displayed the highest BET surface area. The S_{BET} value decreased with

the increase of Ca and Ce ratio. The decreasing BET value is more between CaCe-11 and CaCe-21 compared to between CaCe-21 and CaCe-31. With increasing the Ca/Ce ratio, the average pore volume decreased. The pore size distribution of CaCe-11, CaCe-21 and CaCe-31 are presented in Fig. 1C. The support CaCe-21 exhibited a rather broad range in pore size distribution. The CaCe-11 and CaCe-31 supports had a smaller range of pore sizes.

After the addition of cobalt on the prepared supports observed not much change in isotherm and pore-size distribution patterns compared to that of supports. The S_{BET} values of cobalt catalysts lowered than its support. This might be due to pore blockage by metal particles. The surface area decrement is high in 5CoCaCe-11 and 5CoCaCe-31 compared to that of its supports. On other hand, the decrement in S_{BET} is low in case of 5CoCaCe-21 as that of its support. This is caused by the compact aggregation of metal particles in Ca-enriched catalysts, which significantly reduces the overall porosity as a result decrease the surface area. The textural results make it very clear that the Ca/Ce ratio is vital for producing a porous catalyst with a high surface area. It is widely known that a porous structure and a greater surface area may facilitate the diffusion of reactants and the dispersion of metals during catalytic processes.

3.2. X-ray diffraction analysis

The X-ray diffraction (XRD) patterns of prepared supports and supported Co catalysts with different Ca/Ce ratios are displayed in Fig. 2. All samples were analyzed to examine the structural changes caused by varying Ca/Ce ratio. All support materials showed CeO₂ phase [PDF: 00-034-0394]. The additional reflections corresponding to CaCO₃ phase [PDF: 00-005-0586] detected along with the CeO₂ phase specifically in CaCe-21 support. This might be due to more surface CaO species in case of CaCe-21 support which are forming CaCO₃ by exposing to the air. No major changes observed in diffraction patterns after the addition of cobalt to the supports. Similar crystalline phases were observed in all cobalt catalysts compared to that of their corresponding supports. The reflection of cobalt oxide species will appear at 2θ values 42.68, 49.70 and 72.92 [PDF: 00-048-1719]. In Fig. 2B cobalt oxide reflections are not observed. This might be due to crystal size of cobalt oxide lower than the instrument detection limit.

3.3. TPR studies

The TPR patterns of supports exhibited in Fig. S1 and the quantification results of H₂ consumption displayed in Table 1. Based on literature data, CeO₂ TPR profiles show two reduction peaks (Dobosz et al., 2016). A high temperature peak (above 800 °C) typical of the reduction of bulk ceria and a low temperature peak (below 500 °C) attributed to the reduction of surface ceria. Because of the robust Ca–O bond, it was challenging to reduce bulk CaO. However, at a high temperature (610.3 °C) a very slight reduction peak can be seen, which is most likely the result of very minor Ca–O bond reduction on the surface (Sivasangar et al., 2015). All CaO–CeO₂ supports showed two major peaks one at high temperature corresponds to reduction of bulk ceria and the one at lower temperature corresponds to surface ceria. The increasing CaO amount cause changes in the TPR profile of each support that affects the reducibility of CeO₂ and interaction with CaO. The reduction temperature of bulk ceria is shifting towards lower temperature with the increase of calcium. The CaCe-11 support showed two overlapping peaks at 600–700 °C range. In that the lower one might be Ca interacted ceria and the higher temperature peak might be due to reduction of non-interacted bulk ceria. In CaCe-21 support these peaks are overlapped completely indicates CaO amount is sufficient to interact with Ceria. The reduction tem-

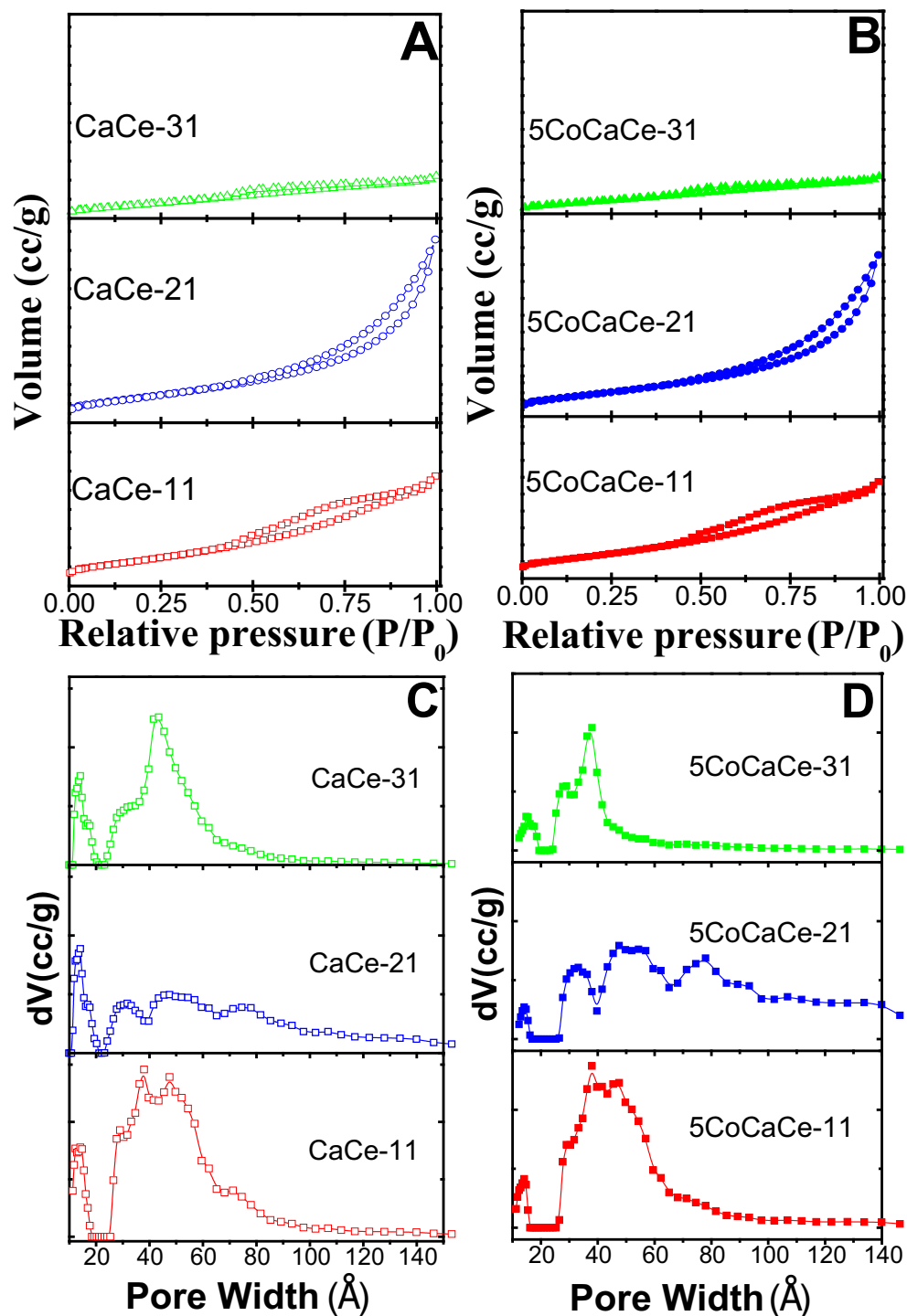


Fig. 1. (A) & (B) Nitrogen adsorption–desorption isotherms, (C) &(D) pore size distribution curves of the calcined supports and catalysts.

perature of bulk ceria moved to a lower temperature in CaCe-31 support. The surface ceria reduction peak observed at low temperature in CaCe-21 compared to that of in CaCe-11 and CaCe-31. The results clearly indicate that Ca/Ce ratio 2 is optimum for good interaction between the components in the support. The H_2 consumption is also higher in CaCe-21 support than other supports (Table 1).

Data from the literature indicate that Co_3O_4 is reduced in two steps: first Co_3O_4 is reduced to CoO ($Co_3O_4 + H_2 \rightarrow 3CoO + H_2O$),

and subsequently to metallic cobalt ($CoO + H_2 \rightarrow Co + H_2O$) (Dobosz et al., 2016). Fig. 3 displays the TPR profiles of cobalt catalysts on $CaO-CeO_2$ oxide with various Ca/Ce ratios. For comparison the TPR profiles of 5 wt% Co on commercial CeO_2 (5Co- CeO_2) and 5 wt%Co on commercial CaO (5Co- CaO) are also presented in Fig. 3. It is clear from Fig. 3 that the reduction temperatures of cobalt oxide are high in case of 5Co- CaO and is reduce at lower temperatures in case 5Co/ CeO_2 catalysts. Three peaks were visible in the TPR pattern of 5CoCaCe-11 catalyst. The first two low tem-

Table 1
Physico chemical properties of CaO-CeO₂ mixed oxides support and Cobalt catalyst with various Ca/Ce ratios.

Catalyst	BET surface area (m ² /g)	Pore volume (cc/g)	Pore width (Å)	H ₂ consumption (μmol/g) ^a	Total basicity (μmol/g) ^b	No. of surface Co (μmol/g) ^c
CaCe-11	110	0.14	37.94	30.45	157.39	–
CaCe-21	76	0.11	14.10	140.94	337.56	–
CaCe-31	71	0.09	43.43	42.04	139.84	–
5CoCaCe-11	76	0.12	37.94	82.39	33.60	30.03
5CoCaCe-21	70	0.13	47.52	311.29	48.19	12.84
5CoCaCe-31	42	0.05	37.94	873.21	10.42	29.96

^a H₂ consumption calculated from 100 to 700 °C range.

^b Total basicity calculated from 100 to 800 °C range.

^c Calculated from CO chemisorption.

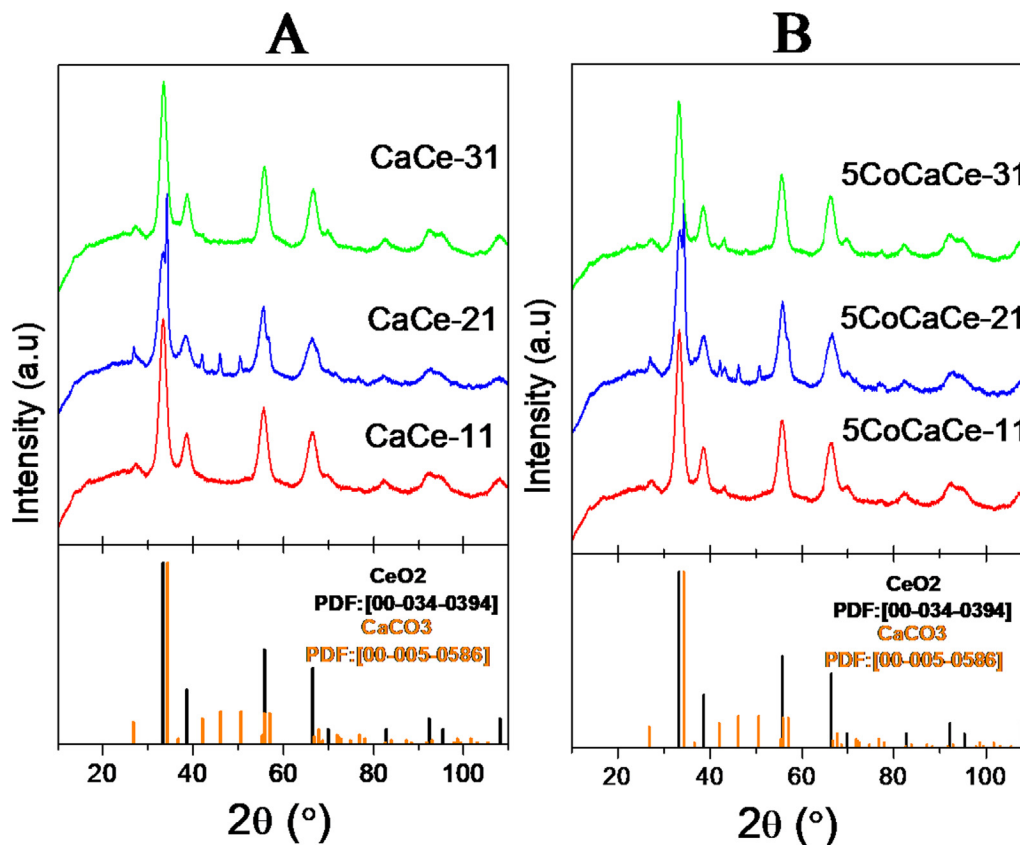


Fig. 2. XRD pattern of calcined (A) Supports and (B) Catalysts.

perature peaks are associated with a two-stage reduction of cobalt oxide below 500 °C, while the third peak is associated with reduction of surface ceria. The 5CoCaCe-11 TPR profile similarly shows a low intense broad peak above 500 °C, which is consistent with the reduction of bulk ceria. The metal reducibility is very low in 5CoCaCe-11 catalyst due to strong metal support interactions. The catalyst 5CoCaCe-21 showed a similar reduction profile as that of 5CoCaCe-11 catalyst, but the peak intensities are high. The H₂ consumption increased in case of 5CoCaCe-21 catalyst compared to that of 5CoCaCe-11 (Table 1), indicates the increased reducibility with increase Ca/Ce ratio. On other hand, at 360 °C, the 5CoCaCe-31 catalyst displayed one big peak with a hump on the lower temperature side. At higher temperatures (>600 °C), no hydrogen consumption was seen. For the catalyst 5CoCaCe-31, there is a discernible improvement in reducibility (Table 1). Earlier, Liotta et al. described this particular behavior (Liotta et al., 2006). They stated that the intimate contact between cobalt oxide and ceria grows with larger cobalt loadings as a result the ceria reducibility

rises. A similar phenomenon is anticipated in 5CoCaCe-31 catalysts, where large concentrations of Co₃O₄ species interact strongly with ceria alone. When compared to the theoretical values needed for the complete reduction of Co₃O₄ to Co, the H₂ consumption (Table 1) for the reduction of catalysts is always higher. This additional H₂ connected to the hydrogen spillover to the support material as well as the partial reduction of ceria.

3.4. Basicity studies

The total basicity of prepared support was analysed by CO₂-TPD measurements. Fig. S2 displays the CO₂ desorption profiles of supports with different Ca/Ce ratio. The quantification results of supports total basicity values are presented in Table 1. The amount of CO₂ desorption was quite high on all CaCe mixed oxide supports. The supports CaCe-11, CaCe-21 and CaCe-31 showed desorption peak with peak maxima at 715, 703 and 681 °C respectively. The outcomes show the existence of strong basic sites. The increasing

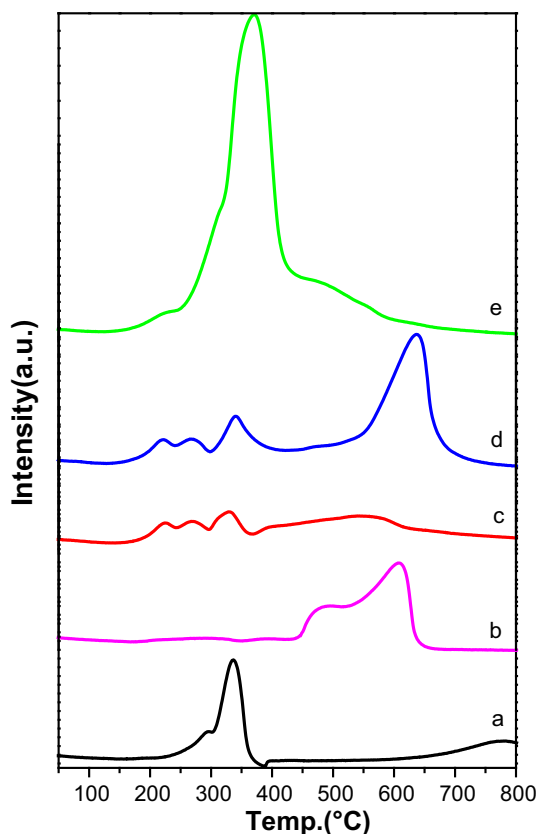


Fig. 3. TPR analysis of calcined cobalt catalysts: (a) 5Co-CeO₂, (b) 5Co-CaO, (c) 5CoCaCe-11, (d) 5CoCaCe-21 and (e) 5CoCaCe-31.

order of basic strength was found to be as follows: CaCe-31 < CaCe-11 < CaCe-21. The improved basicity of the CaCe-21 support is due to synergetic effect between CaO and CeO₂. The CO₂ desorption peak moved to lower temperature with increase of Ca/Ce ratio indicates presence of secondary metal phases CaO in CeO₂ (Teo et al., 2014).

After the addition of cobalt to the supports the strength and distribution of basic sites of the catalysts changed. The total basicity of all catalysts very low compared to that of their corresponding supports (Table 1). This is due to blocking of oxygen in CaO-CeO₂ ion pairs and isolated O²⁻ anions, which are responsible for the Lewis basicity. All catalysts CO₂ TPD patterns showed three different types of desorption peaks, which are shown in Fig. 4. Desorption peaks at low temperatures (below 400 °C) are associated with weak basic sites. Strong basic sites correspond to high temperature desorption peaks, while moderately basic sites correspond to desorption peaks in the 400–600 °C range. All catalysts have more moderate basic sites and catalysts followed similar order of basicity to that of its supports i.e., 5CoCaCe-31 < 5CoCaCe-11 < 5CoCaCe-21.

3.5. Morphology studies

The morphologies of all prepared samples were characterized by SEM analysis. The representative SEM images of support and catalysts are presented Fig. 5. All CaO-CeO₂ supports showed morphology of irregular shaped crystalline agglomerates. There is not much difference observed in all support morphology, but the particle sizes are varied. Low particle size observed in CaCe-21 support than the other supports. With the addition of cobalt to the support, the catalyst morphology changed drastically. The 5CoCaCe-11 cat-

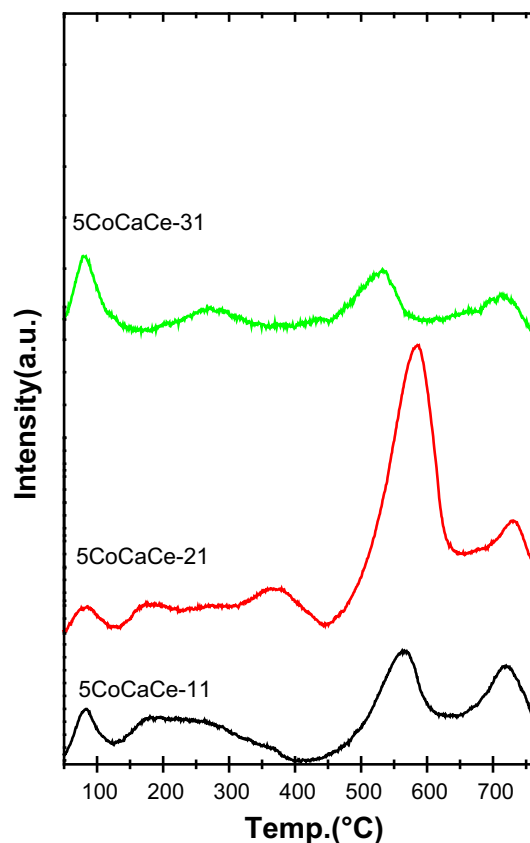


Fig. 4. CO₂ TPD results of cobalt catalysts with different Ca/Ce ratio.

alyst showed bigger agglomerates compared to that of its support. The 5CoCaCe-21 catalyst showed similar morphology as that of its support. The agglomeration increased drastically in 5CoCaCe-31 catalyst where we can clearly see the big lumps of CeO₂ and in Fig. 5. To know the component distribution in the catalyst the elemental mapping performed on several areas of the catalyst and some of the representative images were presented in Fig. 6.

The elemental mapping of 5CoCaCe-11 catalyst in Fig. 6 showed homogenous distribution of Co, Ce and Ca oxides. The results indicate the possibility of strong interactions between metal and support. The TPR results also indicate the strong metal support interaction in 5CoCaCe-11 catalyst. The elemental mapping of 5CoCaCe-21 catalyst in Fig. 6 showed aggregates of CeO₂ and CaO together and cobalt dispersed on both. The elemental mapping of 5CoCaCe-31 catalyst in Fig. 6 showed large lumps of CeO₂ which interact with large amounts of cobalt oxide and calcium oxide is finely dispersed. The SEM results clearly indicate the strong interaction between CeO₂ and Co₃O₄. The TPR results also indicated the strong interaction between CeO₂ and Co₃O₄. The SEM and elemental mapping results are in good agreement with TPR results.

3.6. Catalyst performance studies

The experimental data for the catalytic activity of 5CoCaCe-11, 5CoCaCe-21 and 5CoCaCe-31 catalysts for ammonia decomposition is shown in Fig. 7. For comparison, the activity results of 5Co-CeO₂ (5 wt%Co on commercial CeO₂) and 5Co-CaO (5 wt%Co on commercial CaO) are also displayed in Fig. 7. Because ammonia decomposition is endothermic, the catalysts showed increased activity as the temperature increased (Podila et al., 2015, 2022, Al-attar et al., 2022). From the Fig. 7, the activity of cobalt catalyst on CaO-CeO₂ mixed oxide support is higher than the cobalt catalyst

on individual CaO and CeO₂ supports individually. The results clearly indicate the influence of the support material on the catalyst performance. The cobalt catalyst's activity increased as the Ca/Ce ratio increased, and it achieved the highest conversions at all temperatures with a Ca/Ce ratio of 2. As the Ca/Ce ratio increased further, activity began to decrease. The catalyst 5CoCaCe-21 showed the highest catalytic performance compared to all prepared catalysts. Catalytic activity of all catalysts arranged as follows: 5CoCaCe-21 > 5CoCaCe-31 > 5CoCaCe-11 > 5Co-CeO₂ > 5Co-CaO. Based on repeated experiments, the accuracy for the activity of ammonia decomposition value falls in the error range of $\pm 3\%$.

The high activity of 5CoCaCe-21 catalyst is due to high surface area, easy reducibility and interaction between CaO and CeO₂, which creates synergism between moderate and strong basic sites. An optimum interaction between support and cobalt also might be the reason for high activity. Though the catalyst 5CoCaCe-11 has high surface area and significant basicity (Table 1), showed lower activity compared to other catalyst i.e. 5CoCaCe-21 and 5CoCaCe-31. The main reason for low activity of 5CoCaCe-11 catalyst is strong metal support interaction that resulted low reducibility (Fig. 3 and Table 1).

On other hand, the catalyst 5CoCaCe-31 showed better activity than 5CoCaCe-11 catalyst though it has lower surface area and basicity (Table 1). This is due to strong interaction between Co₃O₄ and CeO₂ (SEM results) which leads to unusual reducibility of catalyst (TPR results). Ca/Ce = 2 ratio is optimal for CaO-CeO₂ mixed oxide support, which affects the physicochemical properties of the cobalt catalyst and increases the decomposition of ammonia.

Fig. 8 shows the apparent activation energies (E_a) of prepared catalysts based on Arrhenius plots ($\ln(k)$ vs. $1/T$) for ammonia decomposition at temperatures ranging from 400 to 550 °C at

6000 h⁻¹ GHSV. The increasing order of E_a for these catalysts was 5CoCaCe-21 < 5CoCaCe-31 < 5CoCaCe-11 correlating well with their catalytic activity. In the present study, we observed catalyst basicity changed by the increase of Ca amount in Ca-Ce mixed oxide and the optimum Ca/Ce ratio in support material will change the electron donating ability to active metal. According to these observations, a suitable amount of calcium in the support will promote ammonia decomposition catalysis. Out of all prepared catalysts, the 5CoCaCe-21 catalyst displayed the lowest E_a value.

To know the exact activity pattern on per site of active metal in cobalt catalysts with different Ca:Ce ratio, plotted a graph between TOF and catalysts with different Ca:Ce ration. The results were displayed in Fig. 9. The number of active cobalt sites in all catalysts were calculated from CO chemisorption results (Table 1). From the results the number of surface cobalt sites are more in 5CoCaCe-11 and 5CoCaCe-31 catalysts compared to that of 5CoCaCe-21 catalyst. The high surface and Co-Ce strong interactions properties are responsible for higher surface cobalt sites. Though the number of surface Co atoms are low in 5CoCaCe-21 catalyst the TOF value is four times higher than the other catalysts. The higher TOF on 5CoCaCe-21 catalyst is indeed due to the high basic character of CaCe-21 support. The beneficial role of support basicity for ammonia decomposition is already reported in literature (Yin et al., 2004b).

3.7. Effect of metal loading

Catalysts with different cobalt loadings on CaCe-21 support were prepared and activities are measured to determine the optimal cobalt content. The results are presented in Fig. 10A. At 300 °C temperature the activity variation over different cobalt

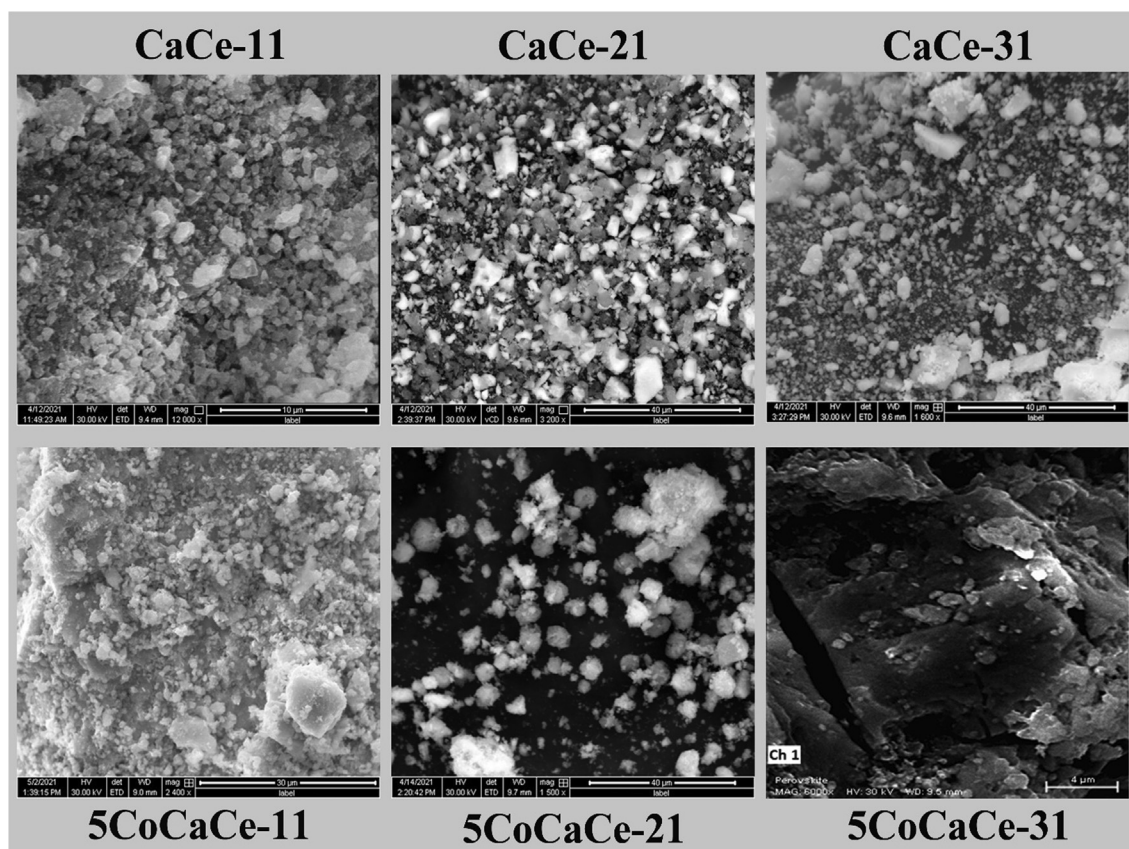
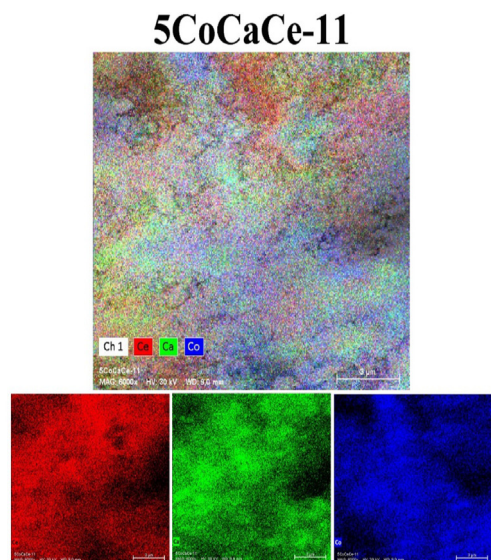
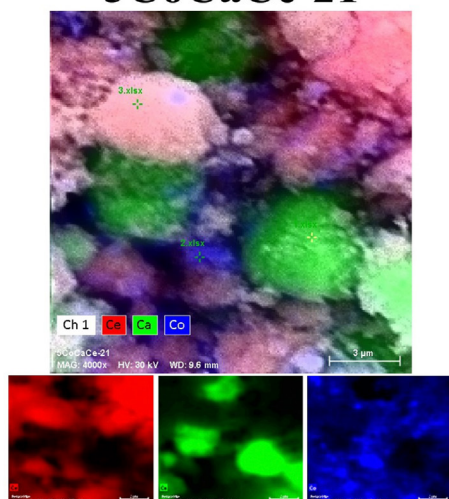


Fig. 5. SEM images of calcined supports and catalysts with different Ca/Ce ratios.



5CoCaCe-21



5CoCaCe-31

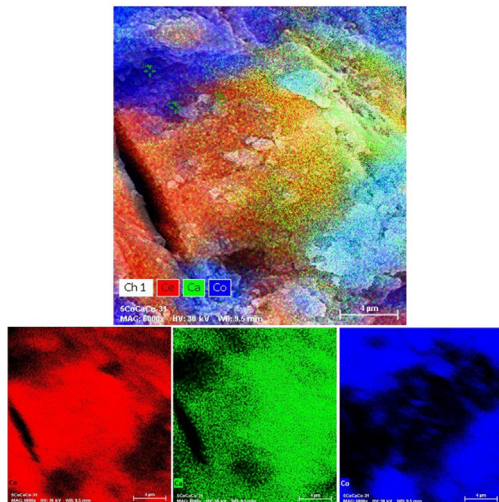


Fig. 6. Elemental mapping of calcined cobalt catalysts.

loadings is difficult to understand because NH₃ conversions are very low. Similarly, at 600 °C catalysts with all cobalt loadings showed almost complete NH₃ conversion.

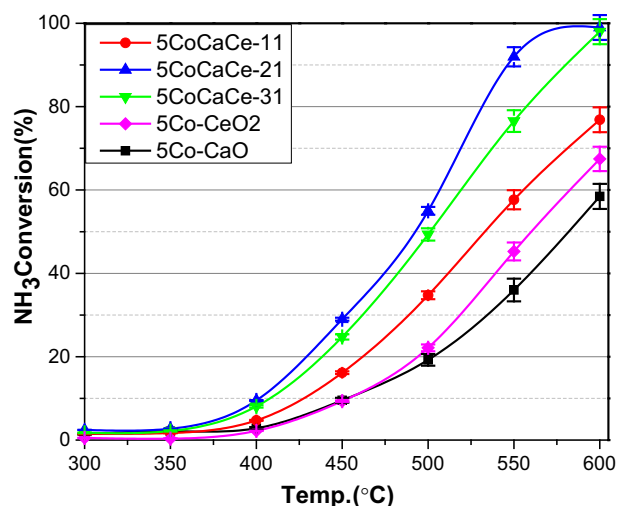


Fig. 7. Ammonia conversion for ammonia decomposition over cobalt catalysts. Reaction conditions; NH₃: 100 vol%, GHSV: 6000 h⁻¹. Activity results are reproducible within ±3% error.

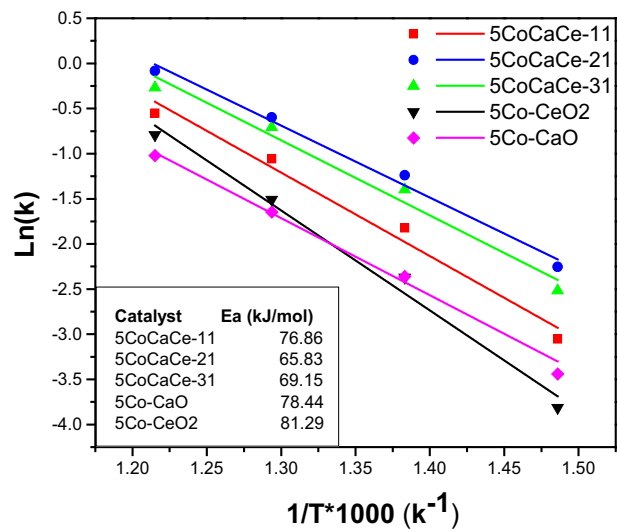


Fig. 8. Arrhenius plots for ammonia decomposition over cobalt catalysts.

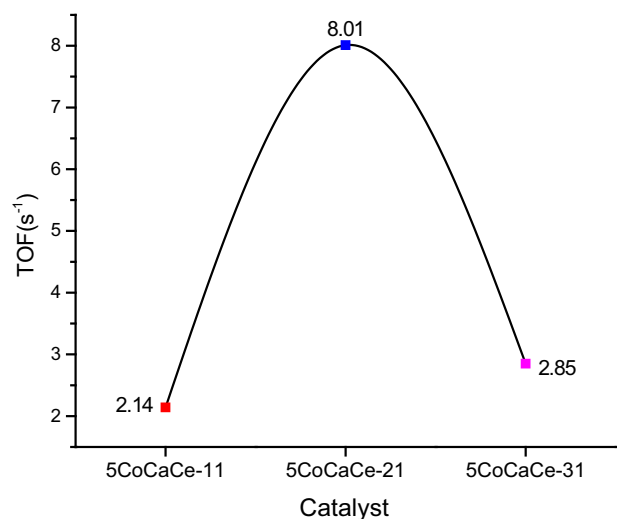
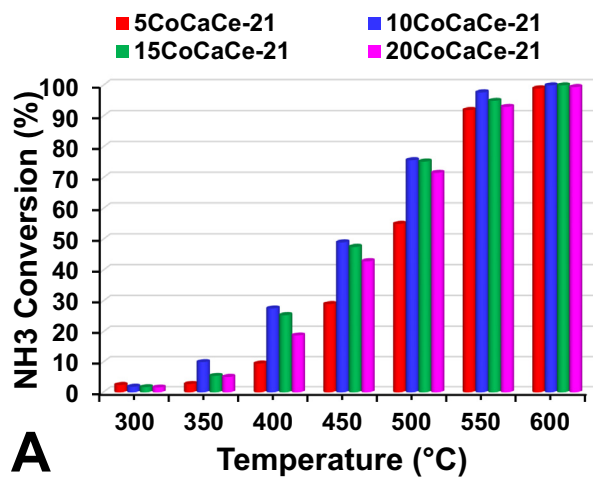
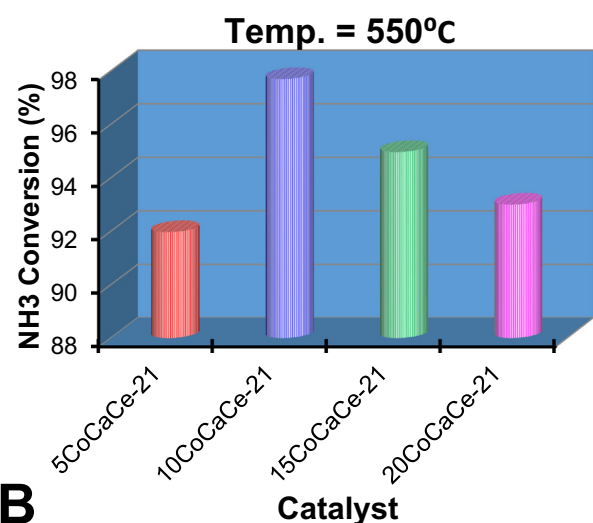


Fig. 9. Variation of TOF with CaCe ratio in Cobalt catalysts at 550 °C with 6000 h⁻¹. TOF = [H₂ formation (μmol/g/sec)]/[Co on surface μmoles/g] Cobalt on surface was calculated from CO chemisorption results.



A



B

Fig. 10. Catalytic performance of cobalt catalysts with different cobalt mass at 6000 h⁻¹ GHSV: (A) at a temperature range 300–600 °C range, (B) at 550 °C.

The activity variation over different cobalt loadings is clear in 350–550 °C. As cobalt content increases in the catalyst, the catalytic activity increases, and 10 wt% cobalt displayed the highest activity, followed by NH₃ conversion decreasing with further increase of cobalt content. This might be caused by the formation of big sized cobalt particles as the cobalt content is higher than

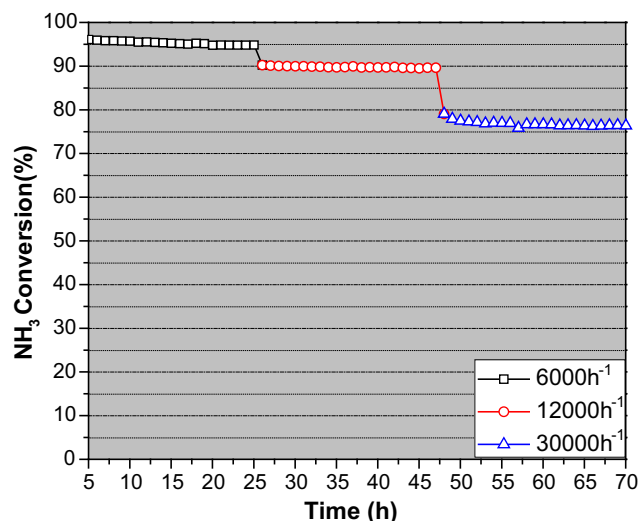


Fig. 11. Stability performance over 10 wt% Co/CaCe-21 catalyst at 550 °C and at different GHSVs.

10 wt%. In addition to the catalyst performance, the stability of the catalysts is another crucial characteristic in practical application. The time on stream study was carried out on 10CoCaCe-21 catalyst using various GHSVs for 70 h at 550 °C. The stability results are displayed in Fig. 11. At all the measured GHSVs, no noticeable activity loss observed. An approximate 95.6% of NH₃ conversion at 6000 h⁻¹, 90.1% of NH₃ conversion at 12000 h⁻¹ and 76.4% of NH₃ conversion at 30000 h⁻¹ observed over 10CoCaCe-21 catalyst at 550 °C. The H₂ formation of different catalysts prepared in this work compared with the cobalt-based and nickel-based catalysts. The results are presented in Table 2. The cobalt-based catalysts developed in this work showed higher activity compared to that of the majority of the catalysts reported in the literature for the generation of hydrogen from NH₃ (Yu et al., 2020, Deng et al., 2012, Gu et al., 2015, Wu et al., 2022). These catalysts are low in price and easy to prepare thus attractive in case of their commercial application.

4. Conclusions

The results concluded that CaO-CeO₂ mixed oxide is promising support for ammonia decomposition reaction. The Ca/Ce ratio greatly influenced the catalyst's activity. Among all prepared cobalt catalysts with different Ca/Ce ratio, 5CoCaCe-21 catalyst is very

Table 2
Comparison of H₂ production results on Co/Ni catalysts from NH₃ at 550 °C.

Catalyst	E _a (kJ/mol)	H ₂ formation rate (mmol/g _{cat} /min)	GHSV (ml/g/h)	Ref.
5% Co/CaCeO-21	65.8	6.16	6000	Present work
10% Co/CaCeO-21	39.5	6.54	6000	Present work
15% Co/CaCeO-21	41.04	6.36	6000	Present work
20% Co/CaCeO-21	49.44	6.23	6000	Present work
5% Co/CeO ₂ -3DOM	64.7	4.2	6000	Huang et al. (2020)
5% Co/MgCeO ₃	76.86	3.86	6000	Al-attar et al. (2022)
5% Co/BaCeO ₃	70.08	5.4	6000	Al-attar et al. (2022)
10% Ni/CeO ₂ -rods	83.8	13.4	30,000	Chen et al. (2022)
5% Ni/CeO ₂	71	6.51	9000	Deng et al. (2012)
5%Co/CNTs	92.0	12.0	36,000	Yu et al. (2020)
90%Co/Al	123.0	33.0	60,000	Gu et al. (2015)
5%Co/Mg-La	67.0	6.0	6000	Podila et al. (2016a,b)
40%Ni/SBA-15	134.7	30.13	30,000	Wu et al. (2022)

efficient for H₂ production from ammonia. Thus Ca/Ce = 2 is optimum ratio for NH₃ decomposition. The enhanced activity of catalyst with Ca/Ce = 2 is due to higher basicity of support (CaCe-21). The morphology and suitable metal support interactions in 5CoCaCe-21 are also possible factors for the effective performance in catalytic activity. The easily reducible Co species, high surface area, and high basicity of the 5CoCaCe-21 catalyst have all been suggested as contributing factors to its increased activity. The effect of cobalt loadings on CaCe-21 was also examined, and found that a 10 wt% cobalt loading is excellent for NH₃ decomposition process. The 10CoCaCe-21 catalyst is highly stable for 70 h of period and very active even at high space velocities.

Declaration of Competing Interest

The authors declare that they have no known competing financial interests or personal relationships that could have appeared to influence the work reported in this paper.

Acknowledgements

The Project was funded by Deanship of Scientific Research (DSR) at King Abdulaziz University, Jeddah, under the Grant no. G: 137-135-1443. The authors, therefore, acknowledge with thanks DSR for technical and financial support.

Appendix A. Supplementary material

Supplementary material to this article can be found online at <https://doi.org/10.1016/j.arabjc.2023.105235>.

References

- Al-attar, O.A., Podila, S., Al-Zahrani, A.A., 2022. Preparation and study of XCeO₃ (X: Mg, Ca, Sr, Ba) perovskite-type oxide supported cobalt catalyst for hydrogen production by ammonia decomposition. *Arab. J. Sci. Eng.*, 1–11 <https://doi.org/10.1007/s13369-022-07255-w>.
- Babu, A., Somesh, T.E., Ani Dechamma, C.D., Hemavathi, A.B., Kakarla, R.R., Kulkarni, R.V., Raghu, A.V., 2023. Ternary structured magnesium cobalt oxide/graphene/polycarbazole nanohybrids for high performance electrochemical supercapacitors. *Mater. Sci. Energy Technol.* 6, 399–408. <https://doi.org/10.1016/j.mset.2023.04.002>.
- Cao, C.-F., Wu, K., Zhou, C., Yao, Y.-H., Luo, Y., Chen, C.-Q., Lin, L., Jiang, L., 2022. Electronic metal-support interaction enhanced ammonia decomposition efficiency of perovskite oxide supported ruthenium. *Chem. Eng. Sci.* 117719. <https://doi.org/10.1016/j.ces.2022.117719>.
- Chen, C., Chen, Y., Ali, A.M., Luo, W., Wen, J., Zhang, L., Zhang, H., 2020. Bimetallic Ru-Fe nanoparticles supported on carbon nanotubes for ammonia decomposition and synthesis. *Chem. Eng. Technol.* 43, 719–730. <https://doi.org/10.1002/ceat.201900508>.
- Chen, C., Fan, X., Zhou, C., Lin, L., Luo, Y., Au, C., Cai, G., Wang, X., Jiang, L., 2022. Hydrogen production from ammonia decomposition over Ni/CeO₂ catalyst: Effect of CeO₂ morphology. *J. Rare Earths.* <https://doi.org/10.1016/j.jre.2022.05.001>.
- Deng, Q.-F., Zhang, H., Hou, X.-X., Ren, T.-Z., Yuan, Z.-Y., 2012. High-surface-area CeO₂ZrO₂ solid solutions supported Ni catalysts for ammonia decomposition to hydrogen. *Int. J. Hydrogen Energy* 37, 15901–15907. <https://doi.org/10.1016/j.ijhydene.2012.08.069>.
- Dobosz, J., Hull, S., Zawadzki, M., 2016. Catalytic activity of cobalt and cerium catalysts supported on calcium hydroxyapatite in ethanol steam reforming. *Polish Journal of. Chem. Technol.* 18. <https://doi.org/10.1515/pjct-2016-0049>.
- Gu, Y.-Q., Jin, Z., Zhang, H., Xu, R.-J., Zheng, M.-J., Guo, Y.-M., Song, Q.-S., Jia, C.-J., 2015. Transition metal nanoparticles dispersed in an alumina matrix as active and stable catalysts for CO x-free hydrogen production from ammonia. *J. Mater. Chem. A* 3, 17172–17180. <https://doi.org/10.1039/C5TA04179A>.
- Hafeez, H.Y., Mohammed, J., Suleiman, A.B., Ndikilar, C.E., Sa'id, R.S., Muhammad, I., 2023a. Insights into hybrid TiO₂-g-C₃N₄ heterostructure composite decorated with rGO sheet: A highly efficient photocatalyst for boosted solar fuel (hydrogen) generation. *Chem. Phys. Impact* 6, 100157.
- Hafeez, H.Y., Mohammed, J., Ndikilar, C.E., Suleiman, A.B., Sa'id, R.S., Muhammad, I., 2023b. Synergistic utilization of magnetic rGO/NiFe₂O₄-g-C₃N₄ S-Scheme heterostructure photocatalyst with enhanced charge carrier separation and transfer: A highly stable and robust photocatalyst for efficient solar fuel (hydrogen) generation. *Ceram. Int.* 49, 5269–5278. <https://doi.org/10.1016/j.ceramint.2022.10.045>.
- Huang, C., Yu, Y., Yang, J., Yan, Y., Wang, D., Hu, F., Wang, X., Zhang, R., Feng, G., 2019. Ru/La₂O₃ catalyst for ammonia decomposition to hydrogen. *Appl. Surf. Sci.* 476, 928–936. <https://doi.org/10.1016/j.apsusc.2019.01.112>.
- Huang, C., Yu, Y., Tang, X., Liu, Z., Zhang, J., Ye, C., Ye, Y., Zhang, R., 2020. Hydrogen generation by ammonia decomposition over Co/CeO₂ catalyst: Influence of support morphologies. *Appl. Surf. Sci.* 532. <https://doi.org/10.1016/j.apsusc.2020.147335>.
- Ji, J., Duan, X., Qian, G., Zhou, X., Tong, G., Yuan, W., 2014. Towards an efficient CoMo/γ-Al₂O₃ catalyst using metal amine metallate as an active phase precursor: Enhanced hydrogen production by ammonia decomposition. *Int. J. Hydrogen Energy* 39, 12490–12498. <https://doi.org/10.1016/j.ijhydene.2014.06.081>.
- Ju, X., Liu, L., Zhang, X., Feng, J., He, T., Chen, P., 2019. Highly efficient Ru/MgO catalyst with surface-enriched basic sites for production of hydrogen from ammonia decomposition. *ChemCatChem*.
- Kim, H.B., Park, E.D., 2022. Ammonia decomposition over Ru catalysts supported on alumina with different crystalline phases. *Catal. Today.* <https://doi.org/10.1016/j.cattod.2022.06.032>.
- Li, L., Meng, Q., Ji, W., Shao, J., Xu, Q., Yan, J., 2017. Embedded iron nanoparticles by graphitized carbon as highly active yet stable catalyst for ammonia decomposition. *Mol. Catal.* 442, 147–153. <https://doi.org/10.1016/j.mcat.2017.09.013>.
- Liotta, L., Di Carlo, G., Pantaleo, G., Venezia, A., Deganello, G., 2006. Co₃O₄/CeO₂ composite oxides for methane emissions abatement: relationship between Co₃O₄-CeO₂ interaction and catalytic activity. *Appl. Catal. B* 66, 217–227. <https://doi.org/10.1016/j.apcatb.2006.03.018>.
- Madhavi, J., Prasad, V., Reddy, K.R., Venkata, R.C., Raghu, A.V., 2021. Facile synthesis of Ni-doped ZnS-CdS composite and their magnetic and photoluminescence properties. *J. Environ. Chem. Eng.* 9. <https://doi.org/10.1016/j.jece.2021.106335>.
- Ohtsuka, Y., Xu, C., Kong, D., Tsubouchi, N., 2004. Decomposition of ammonia with iron and calcium catalysts supported on coal chars. *Fuel* 83, 685–692. <https://doi.org/10.1016/j.fuel.2003.05.002>.
- Podila, S., Alhamed, Y.A., AlZahrani, A.A., Petrov, L.A., 2015. Hydrogen production by ammonia decomposition using Co catalyst supported on Mg mixed oxide systems. *Int. J. Hydrogen Energy* 40, 15411–15422. <https://doi.org/10.1016/j.ijhydene.2015.09.057>.
- Podila, S., Driss, H., Zaman, S.F., Alhamed, Y.A., AlZahrani, A.A., Daous, M.A., Petrov, L. A., 2016a. Hydrogen generation by ammonia decomposition using Co/MgO-La₂O₃ catalyst: Influence of support calcination atmosphere. *J. Mol. Catal. A Chem.* 414, 130–139. <https://doi.org/10.1016/j.molcata.2016.01.012>.
- Podila, S., Zaman, S.F., Driss, H., Alhamed, Y.A., Al-Zahrani, A.A., Petrov, L.A., 2016b. Hydrogen production by ammonia decomposition using high surface area Mo₂N and Co₃Mo₃N catalysts. *Cat. Sci. Technol.* 6, 1496–1506. <https://doi.org/10.1039/C5CY00871A>.
- Podila, S., Driss, H., Zaman, S.F., Ali, A.M., Al-Zahrani, A.A., Daous, M.A., Petrov, L.A., 2017. Effect of preparation methods on the catalyst performance of Co/MgLa mixed oxide catalyst for CO_x-free hydrogen production by ammonia decomposition. *Int. J. Hydrogen Energy* 42, 24213–24221. <https://doi.org/10.1016/j.ijhydene.2017.07.112>.
- Podila, S., Driss, H., Zaman, S.F., Ali, A.M., Al-Zahrani, A.A., Daous, M.A., Petrov, L.A., 2020. MgFe and Mg-Co-Fe mixed oxides derived from hydrotalcites: Highly efficient catalysts for CO_x free hydrogen production from NH₃. *Int. J. Hydrogen Energy* 45, 873–890. <https://doi.org/10.1016/j.ijhydene.2019.10.107>.
- Podila, S., Driss, H., Ali, A.M., Al-Zahrani, A.A., Daous, M.A., 2022. Influence of Ce substitution in LaMO₃ (M = Co/Ni) perovskites for CO_x-free hydrogen production from ammonia decomposition. *Arab. J. Chem.* 15. <https://doi.org/10.1016/j.arabjc.2021.103547>.
- Sing, K.S., 1985. Reporting physisorption data for gas/solid systems with special reference to the determination of surface area and porosity (Recommendations 1984). *Pure Appl. Chem.* 57, 603–619. <https://doi.org/10.1351/pac198254112201>.
- Sivasangar, S., Mastuli, M., Islam, A., Taufiq-Yap, Y., 2015. Screening of modified CaO-based catalysts with a series of dopants for the supercritical water gasification of empty palm fruit bunches to produce hydrogen. *RSC Adv.* 5, 36798–36808. <https://doi.org/10.1039/C5RA03430B>.
- Sivashankar, R., Thirunavukkarasu, A., Nithya, R., Madhubala, V., Deepanraj, B., 2022. Karanja oil transesterification using green synthesized bimetallic oxide catalyst, gCaO-CeO₂: Comparative investigations with the monometallic oxide catalysts on the catalytic efficacy and stability. *Fuel* 319. <https://doi.org/10.1016/j.fuel.2022.123711>.
- Sun, S., Jiang, Q., Zhao, D., Cao, T., Sha, H., Zhang, C., Song, H., Da, Z., 2022. Ammonia as hydrogen carrier: Advances in ammonia decomposition catalysts for promising hydrogen production. *Renew. Sustain. Energy Rev.* 169. <https://doi.org/10.1016/j.rser.2022.112918>.
- Teo, S.H., Rashid, U., Taufiq-Yap, Y.H., 2014. Heterogeneous catalysis of transesterification of jatropha curcas oil over calcium-cerium bimetallic oxide catalyst. *RSC Adv.* 4, 48836–48847. <https://doi.org/10.1039/C4RA08471C>.
- Wu, Z.-W., Li, X., Qin, Y.-H., Deng, L., Wang, C.-W., Jiang, X., 2020. Ammonia decomposition over SiO₂-supported Ni-Co bimetallic catalyst for CO_x-free hydrogen generation. *Int. J. Hydrogen Energy* 45, 15263–15269. <https://doi.org/10.1016/j.ijhydene.2020.04.007>.
- Wu, Z.-W., Xiong, J., Wang, C.-W., Qin, Y.-H., 2022. Supporting high-loading Ni on SBA-15 as highly active and durable catalyst for ammonia decomposition

- reaction. *Int. J. Hydrogen Energy*. <https://doi.org/10.1016/j.ijhydene.2022.11.050>.
- Yin, S.F., Xu, B.Q., Wang, S.J., Ng, C.F., Au, C.T., 2004a. Magnesia-carbon nanotubes (MgO-CNTs) nanocomposite: Novel support of Ru catalyst for the generation of CO_x-free hydrogen from ammonia. *Catal. Lett.* 96, 113–116. <https://doi.org/10.1023/b:catl.0000030107.64702.74>.
- Yin, S.F., Xu, B.Q., Zhou, X.P., Au, C.T., 2004b. A mini-review on ammonia decomposition catalysts for on-site generation of hydrogen for fuel cell applications. *Appl. Catal. A* 277, 1–9. <https://doi.org/10.1016/j.apcata.2004.09.020>.
- Yu, P., Wu, H., Guo, J., Wang, P., Chang, F., Gao, W., Zhang, W., Liu, L., Chen, P., 2020. Effect of BaNH, CaNH, Mg₃N₂ on the activity of Co in NH₃ decomposition catalysis. *J. Energy Chem.* 46, 16–21. <https://doi.org/10.1016/j.jechem.2019.10.014>.
- Zaman, S.F., Jolaoso, L.A., Podila, S., Al-Zahrani, A.A., Alhamed, Y.A., Driss, H., Daous, M.M., Petrov, L., 2018. Ammonia decomposition over citric acid chelated γ -Mo₂N and Ni₂Mo₃N catalysts. *Int. J. Hydrogen Energy* 43, 17252–17258. <https://doi.org/10.1016/j.ijhydene.2018.07.085>.